DOE/ET-53088-316 IFSR #316

A Study of Runaway Electron Confinement in the ASDEX Tokamak

O. J. Kwon and *P. H. Diamond*

Institute for Fusion Studies
The University of Texas at Austin
Austin, Texas 78712

F. Wagner, G. Fussmann, and the *ASDEX* and *NI* Teams

Max-Planck Institut für Plasmaphysik
EURATOM Association
D-8046 Garching bei München, West Germany

March 1988

A Study of Runaway Electron Confinement in the ASDEX Tokamak

O. J. Kwon and P. H. Diamond †

Institute for Fusion Studies, The University of Texas at Austin, Austin, TX 78712

F. Wagner, G. Fussmann, and the ASDEX and NI Teams

Max-Planck-Institut für Plasmaphysik – EURATOM Association,

*D-*8046 *Garching bei München, West Germany*

Abstract

The results of runaway electron confinement experiments from ASDEX are analyzed to elucidate the structure of electromagnetic turbulence that causes anomalous electron heat transport in the L-mode confinement regime. From a simple model, the radial correlation length (W) of the magnetic turbulence is determined to be about 1 mm. Using this value and that of the experimentally deduced electron thermal diffusivity, we determine the radial magnetic fluctuation level at the plasma edge in the L-mode to be $(\widetilde{B}_r/B_0) \sim 2 \times 10^{-4}$. Scalings of W and $\widetilde{B}_r/B_0$ are deduced from parameter scans. From a comparision of these results with the predictions of various theoretical models, it is concluded that skin-depth turbulence, electromagnetic drift wave turbulence, rippling modes, and microtearing modes are inferior candidates and that resistive-ballooning modes offer the best possibility for a consistent interpretation of the data.

---

† Present address: *Department of Physics, University of California, San Diego, La Jolla, CA 92093 and G. A. Technologies, Inc., La Jolla, CA 92138*

I. Introduction

It is well known[1] that the electron thermal diffusivity in tokamaks is much larger than that predicted by neoclassical theory.[2] Magnetic microturbulence is often suggested as the cause of this anomalous transport,[3] since even very small levels of magnetic flutter[4] can destroy magnetic flux surfaces, thus leading to enhanced transport. The resulting electron thermal diffusivity, χ_e, due to stochastic magnetic fields has been calculated in various regimes,[3,5,6] with the use of simple models for the structure of magnetic turbulence. However, the actual source and structure of magnetic fluctuations are not well understood. Here we report on the use of runaway electrons (REs) to elucidate the nature of magnetic turbulence. Such experiments are motivated by the high sensitivity of REs to magnetic flutter.[7,8] It was shown in Ref. 7 that when RE drift effects were considered and a perpendicular correlation length was assumed, theoretical predictions for the RE confinement time (τ_R) and the global energy confinement time (τ_E) could be reconciled with the experimental results for moderate levels of magnetic turbulence. In this paper, we report on the results of experiments in the ASDEX tokamak which used REs as a probe to study the structure of magnetic turbulence that appears to be responsible for both τ_E and τ_R in L-mode confinement regimes. Using a simple, generalized expression for the χ_e for runaway and thermal electrons, we can determine the radial correlation length (W) of the magnetic turbulence from the experimentally determined ratio of τ_E/τ_R. This, in turn, is used to estimate magnetic turbulence levels.

In ASDEX discharges, REs evolve through three different phases: production, acceleration, and loss. First, during the initial discharge phase, when the breakdown voltage is $8-10$ V, REs are produced throughout the plasma, since the electron temperature (T_e) and the density (n_e) profiles are flatter than those later in the discharge. The generation of REs greatly diminishes after 60 ms, since the loop voltage drops below 1.5 V, so that $E < E_D/30$, where E_D is the Dreicer electric field.[9] That the production of REs is no longer significant is further confirmed by sequential beam firing experiments. In the second

phase, during the current ramp-up (typically $600 - 800$ ms), REs are no longer generated but are continuously accelerated. Finally, after about 1 second, the current plateau phase begins. This phase is characterized by a steady state RE distribution at a mean energy of about 1 MeV. In this phase, REs are continuously lost due to turbulent transport.

REs are detected using measurements of thick target, hard X-ray bremsstrahlung (ϕ_x). A characteristic time for the exponential decrease of ϕ_x during the plateau phase can be interpreted as τ_R, since the population and the energy distribution of REs are invariant during this period. In ohmically heated plasmas (OH-mode), τ_R is generally a few hundred ms, while τ_E is $80 - 90$ ms. It is worthwhile to note here that τ_R is strongly influenced by a change of magnetic field topology at the plasma periphery; i.e., a sharp degradation of τ_R, accompanied by strong modulation of ϕ_x by sawtooth activity, is observed when q_a is near 3, where q_a is the value of the safety factor at the edge. However, the bulk plasma is insenstive to such variations.

During neutral beam injection (NBI), ϕ_x surges upward and then decreases very sharply, corresponding to a deterioration in RE confinement. This deterioration is accompanied by a degradation in τ_E and in the particle confinement time (τ_P), even at low beam power. Unlike the OH-mode case, there is no additional drop in τ_R when a rational q_a value ($q_a = 3$) is passed through. This suggests that the quality of the magnetic field topology has deteriorated, so that the effects of additional perturbations are not so dramatic. Indeed, unlike the OH-mode, sawteeth strongly modulate ϕ_x in the L-mode for *all* q_a values. However, because β_p is low (β_p is the ratio of the kinetic pressure to the poloidal magnetic field pressure), the deterioration of τ_R cannot be trivially attributed to increased sawtooth activity. At the transition from the L-mode to the H-mode,[10] the confinement of REs sharply improves, along with τ_E and τ_P, while β_p also increases due to improved global confinement.

A clear correlation between the confinement properties of the bulk plasma and of the REs suggests that the degradation of τ_E and τ_P in the L-mode is perhaps due

to magnetic turbulence, which is evidently also responsible for RE confinement. There is still doubt whether the OH confinement of the bulk plasma is controlled by magnetic turbulence, since the q_a dependences of τ_R and τ_E are uncorrelated in the OH-mode. However, it is clear that magnetic turbulence is not a trivial consequence of rising β, as predicted by drift wave theory,[11] because of the implication of what is observed at the L→H transition, where β and τ_R both increase.

In the present study, we analyse RE confinement data to probe the structure of magnetic microturbulence. Specifically, we determine the radial correlation length of the underlying magnetic turbulence using a simple model, explained in Sec.III, which clarifies and extends previous work.[6,7,8] Because of the dominant ∇B drift effect, the coupling of REs to microturbulence is greatly reduced, so that the effects of large RE velocity[5] parallel to the equilibrium magnetic field (B_0) are weakened by cross-field drifts. This enables us to calculate W from the ratio of τ_E/τ_R, using the assumptions that energy is lost through the electron conduction channel and that the electron loss channel is controlled by magnetic turbulence in the L-mode. Then, the relative amplitude of magnetic fluctuations ($b_0 = \tilde{B}_r/B_0$) necessary for the stochastic field-induced χ_e to match the expermentally deduced χ_e can also be determined if the spectrum-averaged poloidal mode number ($\overline{m}$) is known. The dependence of W and b_0 on basic plasma parameters, such as the toroidal magnetic field (B_T), the density, and the total input power (P), are determined semi-empirically from experimental scans of τ_E and τ_R with respect to those parameters. Having obtained the values and parametric dependences of W and b_0, we then test the consistency of various microturbulence theories.

The remainder of this paper is organized as follows. In Sec. II, the experimental data is presented. The implications for χ_e and τ_R are discussed. A simple model for χ_e for both thermal and runaway electrons, including drift and finite Larmor radius effects, is derived in Sec. III. In Sec. IV, the results obtained by using the model to analyze the data from ASDEX are compared with the predictions of various theoretical models. Finally,

Sec. V contains a summary and conclusions.

II. Experimental Results

The measurements described below were performed on ASDEX, a diverted tokamak with major radius $R = 165$ cm and minor radius $a = 40$ cm. Discharges cover the parameter range of $B_T = 2.0 - 3.0$ T, plasma current $I_p = 200 - 400$ kA, loop voltage $V_L = 0.5 - 1.5$ V, and $n_e = 4 - 8 \times 10^{13}$ cm^{-3}.

The RE drift orbit is shifted outward with respect to the magnetic field lines (Fig. 1), because the guiding-center velocity of REs has both a poloidal (θ) component, due to the helical motion around the magnetic axis, given by

$$v_\theta = v_\parallel \frac{B_p}{B_T}, \tag{1}$$

(where B_p is the poloidal magnetic field), and a vertical component, due to curvature and ∇B drifts, given by

$$v_D = \frac{1}{\Omega_e R}\left(v_\parallel^2 + \frac{1}{2}v_\perp^2\right), \tag{2},$$

where $\Omega_e = eB_T/\gamma m_e c$ is the electron gyrofrequency and γ is the relativistic factor. The orbit displacement ΔR is determined by tracking v_θ and v_D. When $a \gg \Delta R$, we have

$$\Delta R \simeq \frac{m_e c^2}{eB_T}\overline{q}\sqrt{\gamma^2 - 1}, \tag{3}$$

where $\overline{q}$ is the average q value along the trajectory. When this orbit intersects a molybdenum target placed at the plasma midplane a few centimeters outside the separatrix on the low-field side, hard X-rays are emitted.

In Fig. 2, ϕ_x is measured during the OH-mode interrupted by two sequential NBI pulses. During the first NBI phase, ϕ_x decreases very rapidly, indicating that REs are quickly lost due to strong magnetic turbulence. However, the second NBI pulse has little effect on ϕ_x because REs are already almost gone and there has been no significant generation since the first pulse. This result, along with the fact that the electric field inside the plasma is much smaller than E_D, confirms the assumption that most REs are generated during the discharge initiation phase, especially before 60 ms. Also, a steady-state energy

distribution of REs seems to develop during the plateau phase, since the acceleration of high energy REs greatly diminishes compared to "free-fall" acceleration during this phase. Because of these characteristics and because the variation of ϕ_x is roughly exponential, the e-folding time of ϕ_x is a good measure of τ_R, even if there may be some corrections due to weak generation and acceleration processes.[12] It is worthwhile to note that these corrections have little effect on results.

Figure 3(a) shows I_p and the central chord-averaged electron density, $\overline{n}_e$, during the initial and current ramp-up phases. The corresponding ϕ_x is shown in Fig. 3(b). In the current ramp-up phase, ϕ_x increases, not because more REs are generated, but because REs continuously gain energy. The sequence of rational q surfaces moves from the interior across the separatrix as I_p is ramped up, with τ_R being degraded as each rational q_a is crossed. The quality of the magnetic field configuration is not influenced by the presence of the separatrix, but rather by the cylindrical q_a value.

In ohmic discharges, RE confinement is strongly affected by q_a whereas bulk plasma confinement is not, as shown in the B_T scan of Fig. 4. A sharp degradation of τ_R is observed at $q_a \simeq 3$, where ϕ_x is strongly modulated by sawteeth. Away from $q_a \simeq 3$, little or no modulation of ϕ_x is observed. Other known global quantities, such as τ_E in Fig. 4, are almost completely insensitive to the destruction of the magnetic field topology at the plasma periphery.

NBI applied during the ohmic plateau phase causes a very sharp decrease in ϕ_x (Fig. 5(b)), as compared to the case without NBI (Fig. 5(a)). This corresponds to a sharp reduction in τ_R, leading to almost full depletion of the RE population in a very short period of time. In the L-mode, strong modulation of ϕ_x by sawteeth is observed for all q_a values (Fig. 5(b)), but in the OH-mode, only for rational q_a-values. The turbulence that causes anomalous transport in the L-mode affects all three confinement properties (τ_E, τ_P, and τ_R) simultaneously (Fig. 6) and increases with higher neutral beam power (P_{NI}). Both τ_R and τ_E decrease monotonically from their values in the OH-mode with

increasing P_{NI} and approach 100 ms and 20 ms, respectively, when P_{NI} reaches a few megawatts. In all cases, τ_R remains $5-10$ times greater than τ_E. The sharp drop in τ_R at low P_{NI} indicates that a substantial degradation of magnetic field topology occurs at very low P_{NI}. It also indicates that sawtooth coupling does not play a significant role in τ_R. This suggests that in the case of ASDEX, at least, the L-mode is not a mere continuation of the OH-mode, but rather that a different mechanism is triggered by NBI. During NBI, τ_R increases monotonically with q_a in a B_T scan (Fig. 7), unlike the case of the OH-mode, where sharp degradations at rational q_a values are observed (Fig. 4). The high sensivity of REs to magnetic turbulence indicates that NBI degrades the quality of the magnetic field configuration to such an extent that the additional disturbance caused by a rational q_a surface is barely observable. The bulk plasma is insensitive to rational q_a values, as in the OH-mode.

Figure 8 shows sequential traces for ϕ_x, $\overline{n}_e$, H_α-radiation, and ϕ_a, for OH-, L-, and H-modes. The H_α-radiation and ϕ_a are measures of the energy flux and the particle flux into the divertor, respectively. It is interesting to note that although the three signals (ϕ_x, H_α, and ϕ_a) are governed by different transport properties (i.e., RE, heat transport and particle transport), they show simultaneous OH→L and L→H transitions. Especially at the L→H transition, the rapid increase in τ_R, characterized by the discontinuity in ϕ_x' (the time derivative of ϕ_x), tracks the increase in τ_E and τ_P.

It is clear from correlations between the confinement properties of REs and the bulk plasma in the L-mode that the confinement properties of both may be governed by magnetic turbulence. By analyzing data presented in this section, we can extract some useful information about the structure of magnetic microturbulence, mainly, W and b_0. The scaling dependence of W and b_0 on P and q_a (or equivalently on B_T) can be determined from analyses of Figs. 6 and 7, respectively. The results of the scans of $\overline{n}_e$, which are used to determine the parametric dependence of τ_R and τ_E on $\overline{n}_e$ in the OH- and L-modes, are presented in Fig. 9, where τ_E increases with $\overline{n}_e$, while τ_R decreases with $\overline{n}_e$ for moderate

beam power ($P_{NI} = 0.4$ MW).

III. Generalized Theory of Electron Thermal Diffusivity

In this section, a simple model for χ_e due to stochastic magnetic field is set forth. An attempt is made to relate τ_E and τ_R, which are global quantities, to local values of χ_e that are determined from local estimates of microinstability-induced transport.

A. Electron Thermal Diffusivity

To derive an expression for χ_e that is applicable to REs as well as thermal electrons, the electron drift kinetic equation[13] is used:

$$-i\left(\omega-\omega_D-k_\parallel v_\parallel\right)\tilde{g}_{\mathbf{k},\omega}+\sum_{\mathbf{k}',\omega'} v_\parallel \tilde{\mathbf{b}}_{\mathbf{k}',\omega'}\cdot\nabla\tilde{g}_{\mathbf{k}-\mathbf{k}',\omega-\omega'}=-v_\parallel\tilde{b}_{r,\mathbf{k},\omega}\frac{\partial f_0}{\partial r}J_0\left(k_\perp\rho_e\right). \quad (1)$$

Here, $\tilde{g}_{\mathbf{k},\omega}$ is the nonadiabatic part of the fluctuating electron distribution function, ω is the mode frequency, $k_\parallel$ is the wavenumber parallel to the magnetic field, and f_0 is the equilibrium electron distribution function. Also, J_0 is the Bessel function of zeroth order, representing FLR effects, and ρ_e is the electron Larmor radius. A simple slab geometry is used to calculate the drift frequency, ω_D:

$$\omega_D=\frac{k_\theta}{\Omega_e R}\left(v_\parallel^2+\frac{1}{2}v_\perp^2\right), \quad (2)$$

where k_θ is the poloidal wavenumber. Note that the only nonlinear interaction of $\tilde{g}_{\mathbf{k},\omega}$ in Eq. (1) is with magnetic flutter, $\tilde{\mathbf{b}}_{\mathbf{k},\omega}$, normalized to B_T. This nonlinear term is simplified as

$$\sum_{\mathbf{k}',\omega'} v_\parallel \tilde{\mathbf{b}}_{\mathbf{k}',\omega'}\cdot\nabla\tilde{g}_{\mathbf{k}-\mathbf{k}',\omega-\omega'}=\frac{1}{\tau_{c\mathbf{k}}}\tilde{g}_{\mathbf{k},\omega}, \quad (3)$$

where $\tau_{c\mathbf{k}}$ is the nonlinear decorrelation time, which is an effective lifetime for scales of order $|\mathbf{k}|^{-1}$. The evolution of f_0 is described by

$$\frac{\partial f_0}{\partial t}=-\frac{\partial\Gamma_p}{\partial r}. \quad (4)$$

Here, Γ_p is the phase space flux, given by

$$\Gamma_p=v_\parallel\sum_{\mathbf{k},\omega}\tilde{b}_{r,-\mathbf{k},-\omega}J_0(k_\perp\rho_e)\tilde{g}_{\mathbf{k},\omega}. \quad (5)$$

It is easy to see that Eq. (4) is a diffusion equation with diffusion coefficient determined from Eqs. (1), (3), and (5) as

$$\chi_e = v_\parallel^2 \sum_{\mathbf{k},\omega} |\tilde{b}_{r,\mathbf{k},\omega}|^2 J_0^2(k_\perp \rho_e) \mathrm{Re}\left[i \left(\omega - \omega_D - k_\parallel v_\parallel + \frac{i}{\tau_{ck}} \right)^{-1} \right], \tag{6}$$

where Re$[\cdots]$ denotes the real part of $[\cdots]$.

In the quasilinear approximation, where we neglect nonlinear mode coupling, Eq. (6) becomes

$$\chi_e = \pi v_\parallel^2 \sum_{\mathbf{k},\omega} |\tilde{b}_{r,\mathbf{k},\omega}|^2 J_0^2(k_\perp \rho_e) \delta(\omega - \omega_D - k_\parallel v_\parallel). \tag{7}$$

When the ballistic frequency, $k_\parallel v_\parallel$, is dominant over ω and ω_D, and FLR effects are ignored, then χ_e further reduces to

$$\chi_e = \pi |v_\parallel| \sum_{\mathbf{k},\omega} |\tilde{b}_{r,\mathbf{k},\omega}|^2 \delta(k_\parallel). \tag{8}$$

It is interesting to note that Eq. (8) is equivalent to the expression for χ_e derived in Ref. 5, since $k_\parallel$ can be also written as $(n - m/q)/R$, where n and m are the toroidal and the poloidal mode numbers, respectively. However, this simple expression for χ_e leads to the conclusion that $\tau_R \ll \tau_E$ (because of the very large $v_\parallel$ of REs), in contradiction with experimental results from ASDEX, where $\tau_R \simeq (5 \sim 10)\tau_E$ (see Fig. 6), and elsewhere.[7] This discrepancy can be resolved[7,8] when the full expression for χ_e is considered.

B. Magnetic Fluctuation Spectrum

In this section, we specify the structure of the radial magnetic field fluctuations and make a few simplifications in order to evaluate the right-hand side of Eq. (6). The first simplification can be made if one notes that magnetic fluctuations that contribute to χ_e are due to microturbulence excited near a rational surface and localized in radius. For a continuum of localized modes, we can write

$$\sum_{\mathbf{k}} = \sum_m \sum_n \simeq \int dm \frac{|q'|}{q^2} |m| \int dx, \tag{9}$$

where $q' = dq/dr$ and x is the radial displacement from the rational surface. With this change, it is also convenient to describe $\tilde{b}_r$ in terms of m and x, i.e.,

$$|\tilde{b}_{r,\mathbf{k},\omega}|^2 = |\tilde{b}_{r,m,n,\omega}|^2 = C^M F(m) S_{\mathbf{k},\omega}\left(\frac{x}{W_m}, \omega\right). \tag{10}$$

Here, $F(m)$ is a poloidal mode number distribution function, W_m is the radial correlation length for mode m, and $S_{\mathbf{k},\omega}$ is a radial structure function. The constant C^M is chosen to give the mean-square amplitude of the magnetic fluctuation level, i.e.,

$$b_0^2 = \sum_{\mathbf{k},\omega} |\tilde{b}_{r,\mathbf{k},\omega}|^2, \tag{11}$$

and therefore

$$C^M = b_0^2 \left[\frac{|q'|}{q^2} \int dm |m| W_m F(m)\right]^{-1}. \tag{12}$$

Separating the frequency spectrum from $S_{\mathbf{k},\omega}$ in Eq. (10) yields

$$|\tilde{b}_{r,\mathbf{k},\omega}|^2 = \frac{b_0^2}{W_{mI} I} F(m) S_{\mathbf{k}}\left(\frac{x}{W_m}\right) \frac{\Delta\omega_{\mathbf{k}}}{\pi\{(\omega - \omega_{\mathbf{k}})^2 + \Delta\omega_{\mathbf{k}}\}}. \tag{13}$$

Here, $\Delta\omega_{\mathbf{k}}$ is the line width of the frequency spectrum; $I = (|q'|/q^2) \int dm |m| F(m)$; and W_{mI} normalizes $S_{\mathbf{k}}$ such that

$$\frac{1}{W_{mI}} \int dx S_{\mathbf{k}}\left(\frac{x}{W_m}\right) = 1, \tag{14}$$

with $S_{\mathbf{k}}(0) = 1$.

From Eqs. (9) and (14), one can easily evaluate the right-hand side of Eq. (8), which yields

$$\chi_e \simeq \frac{\pi |v_\parallel| L_s b_0^2}{\overline{k}_\theta \overline{W}_{mI}}, \tag{15}$$

where $L_s = Rq/\hat{s}$ is the shear length and $\hat{s} = rq'/q$ is the shear parameter. Thus the effective connection length, denoted as D_{st} in Ref. 5, is identified as $\pi L_s b_0^2 / \overline{k}_\theta \overline{W}_{mI}$, where $(\overline{\cdots})$ denotes the spectrum average. One can now experimentally estimate χ_e for the bulk plasma if b_0, $\overline{W}_{mI}$, and $\overline{k}_\theta$ (or $\overline{m}$) are measured.

C. Basic Scales and Regimes

The estimation of χ_e is further simplified, without loss of generailty, if χ_e is evaluated in two different regimes, separated according to different time scales. Autocorrelation times (τ_{ac}) are related to the natural randomization time of the spectrum. These are $|v_D \Delta \mathbf{k}|^{-1}$ (due to the spread in wavenumber, $\Delta \mathbf{k}$), $\Delta \omega_{\mathbf{k}}^{-1}$ (due to the spread in frequency spectrum), and $|k'_\parallel v_\parallel W_{\mathbf{k}}|^{-1}$ (the wave-electron decorrelation time). Usually, one can take

$$\tau_{ac} = (k'_\parallel |v_\parallel| W_{\mathbf{k}})^{-1}, \tag{16}$$

since it is the fastest of the three time scales. The correlation time (τ_c) is the turbulent decorrelation time, determined under the assumptions that dominant length scale causing anomalous transport is $W_{\mathbf{k}}$ and that the dominant time scale is τ_c, i.e.,

$$\tau_c = \left(\frac{\chi_e}{W_{\mathbf{k}}^2} \right)^{-1}. \tag{17}$$

In the 'strong' turbulence regime, where $\tau_c < \tau_{ac}$, turbulence is fully developed and the nonlinear interaction between different modes becomes dominant. In the 'weak' turbulence regime, $\tau_{ac} < \tau_c$ and nonlinear interactions can be neglected.

D. Comparision of χ_e for Thermal and Runaway Electrons

In this section, we evaluate χ_e (Eq. (6)) for thermal and runaway electrons in both the strong and the weak turbulence regimes. These are compared in order to obtain W. The magnitude of b_0 can also be estimated so as to match the experimentally observed value of χ_e when $\overline{m}$ is known.

For thermal electrons in the weak turbulence regime, χ_e is given by Eq. (15). For thermal electrons in the strong turbulence regime, χ_e can be calculated from Eqs. (6), (9), (13), (14), and (17) to yield

$$\chi_{e,Th} = |v_\parallel|_{Th} b_0 W, \tag{18}$$

where the subscript 'Th' is added to indicate thermal electrons. Thus, in this regime the effective connection length for thermal electrons (D_{st}) is $b_0 W$. Comparing Eqs. (15) and (18), one can see that the integration constant $\overline{W}_{mI}$ is absent in Eq. (18) because $S_{\mathbf{k}}$ is radially averaged instead of being evaluated at a particular position (at $x = 0$ in Eq. (15)). It is interesting to note that because the dependence of χ_e on b_0 is different in the two regimes, one can experimentally determine the proper regime for thermal electron diffusion.

It is very likely that REs are in the weak turbulence regime because of their large parallel velocity. However, χ_e is not given by Eq. (15) since w_D and $k_\parallel v_\parallel$ are comparable and the Doppler shift away from the $\mathbf{k} \cdot \mathbf{B} = 0$ resonance becomes significant for REs. Therefore, we have

$$\chi_{e,R} = \pi v_{\parallel,R}^2 \sum_{\mathbf{k},\omega} |\tilde{b}_{r,\mathbf{k},\omega}|^2 J_0^2(k_\perp \rho_{e,R}) \delta(\omega_{D,R} - k_\parallel v_{\parallel,R}), \tag{19}$$

where the subscript 'R' denotes runaway electrons. Even for REs, the argument of J_0 is small enough for FLR effects to be ignored. So, with our representation of the magnetic fluctuation spectrum, Eq. (19) yields

$$\chi_{e,R} = \pi |v_\parallel|_R \frac{L_s b_0^2}{k_\theta \overline{W}_{mI}} S_{\mathbf{k}} \left(\frac{\omega_{D,R}}{\overline{k}'_\parallel v_{\parallel,R} W} \right). \tag{20}$$

It is important to note the appearance of $S_{\mathbf{k}}$, representing the significance of the radial excursion of REs, as well as the appearance of $\overline{W}_{mI}$ (instead of W). The X-ray spectrum is expected to cut off at very high energy because the radial excursion width of very high energy REs greatly exceeds W and the argument of $S_{\mathbf{k}}$ becomes so large that $\chi_{e,R}$ eventually vanishes.

Now, we can calculate W by comparing $\chi_{e,Th}$ and $\chi_{e,R}$ and using Fig. 6. For simplicity, we assume that thermal electrons are also in the weak turbulence regime. This assumption is marginally satisfied for ASDEX parameters. From Eqs. (15) and (20), we obtain

$$\frac{\tau_E}{\tau_R} \simeq \frac{\chi_{e,R}}{\chi_{e,Th}} = \frac{v_{\parallel,R}}{v_{\parallel,Th}} S_{\mathbf{k}} \left(\frac{L_s v_{D,R}}{W v_{\parallel,R}} \right). \tag{21}$$

Without the $S_{\mathbf{k}}$ term, Eq. (21) would predict $\tau_R \ll \tau_E$, as in the simple theory.[5] However, $S_{\mathbf{k}}$ evaluated at the radially shifted position for REs becomes smaller than the ratio of $v_{\parallel,R}/v_{\parallel,Th}$, so that τ_R becomes longer than τ_E, consistent with experimental results.

To find W, we need to solve Eq. (21), which requires inversion of the $S_{\mathbf{k}}$ function. The structure of $S_{\mathbf{k}}$ could be understood in detail experimentally, if the τ_R spectrum of RE energy were measured. We consider a simple case here. If $S_{\mathbf{k}}$ is Gaussian, then Eq. (21) yields

$$W = L_s \frac{v_{D,R}}{v_{\parallel,R}} \ln^{-\frac{1}{2}} \left(\frac{v_{\parallel,R} \tau_R}{v_{\parallel,Th} \tau_E} \right), \tag{22}$$

and from Eqs. (15) and (22), we find

$$b_0 = \pi^{-\frac{1}{4}} \left(\frac{\overline{k}_\theta \chi_{e,Th} v_{D,R}}{v_{\parallel,Th} v_{\parallel,R}} \right)^{\frac{1}{2}} \ln^{-\frac{1}{4}} \left(\frac{v_{\parallel,R} \tau_R}{v_{\parallel,Th} \tau_E} \right). \tag{23}$$

Thus, only τ_W/τ_R and the average energy of the REs need to be measured to determine W. However, $\chi_{e,Th}$ and $\overline{k}_\theta$ (or $\overline{m}$) must also be known in order to determine b_0.

IV. Analysis of Data

Having derived a simple generalized expression of χ_e for the REs and the bulk plasma, we now analyze experimental data from the ASDEX tokamak in order to find the magnitudes and scalings of W and b_0. Noting that the τ_R and τ_E measurements are global, we calculate W and b_0 at the two different radial positions of the plasma that are believed to be related to the overall transport behavior, viz., at the $q = 2$ surface[14] and at the edge[15] of the plasma. The results are shown in Table 1. For the L-mode, a typical neutral beam injection power of 1 MW is chosen. It is worthwhile to note again that in the OH-mode, it is questionable whether the confinement of the bulk plasma is also governed by the magnetic turbulence, since the q_a dependences of τ_R and τ_E are uncorrelated. However, τ_R and τ_E cannot be simultaneously governed by electrostatic turbulence, as shown in the Appendix.

The magnitude of W is insensitive to the theoretical model for $S_{\mathbf{k}}$. Hence, detailed information about the structure of $S_{\mathbf{k}}$ (the τ_R spectrum in terms of the RE energy) is not very important for finding W and b_0. As seen in Table 1, W is also insensitive to the confinement zones and is of order of 1 mm, consistent with the notion that W arises from *micro*turbulence.

With the experimentally deduced radial profile[16] of χ_e and with the choice[17] $6 \leq \overline{m} \geq 10$,it is found that b_0 is larger at the edge than at the $q = 2$ surface, corresponding to radially increasing χ_e. The magnitude of b_0 is also larger in the L-mode than in the OH-mode, corresponding to confinement degradation during auxiliary heating. It is interesting to note that even very weak radial magnetic fluctuations ($b_0 \geq 10^{-4}$) can induce significant anomalous electron heat transport. Furthermore, this level suffices for magnetic field lines to become stochastic, which is a necessary condition for this theory to be valid.

The scaling of W with P (note that P denotes the total power, not just the neutral beam injection power) can be found by analysing Fig. 6. It should be noted here that the ratio of τ_R/τ_E is mostly influenced by W; i.e., when W decreases, the RE drift

effect is enhanced, leading to an increase in τ_R/τ_E and vice versa. Now, since Fig. 6 shows that the responses of τ_R and τ_E to changes in P are quite similar, it can be easily inferred that W is very weakly dependent on P.

However, τ_R and τ_E respond to changes in q_a (or B_T) differently; i.e., τ_R increases with q_a, while τ_E remains constant in the L-mode, making τ_R/τ_E increase with q_a as shown in Fig. 7. This indicates that W decreases as q_a increases, in that the Doppler effect of the REs due to their large radial excursion becomes larger. The inverse scaling of $v_{D,R}$ with B_T makes this dependence even stronger. However, because τ_R/τ_E decreases as n_e increases as shown in Fig. 9, W increases as n_e increases, so that the RE drift effect is suppressed. The parameter scan results can be summarized as

$$W \sim n_e^{0.2} B_T^{-1.3} P^{0.05}. \tag{24}$$

Furthermore, a scaling study of b_0 can be similarly done, although simple inferences are not easily drawn from Figs. 6, 7, and 9 because of rather complicated dependences. The result is given by

$$b_0 \sim n_e^{-0.05} B_T^{-0.6} P^{0.6} \tag{25}$$

We next compare these results with predictions of various microturbulence theories. First, "skin-depth turbulence"[18] whose radial scale length is c/ω_{pe}, where ω_{pe} is the electron plasma oscillation frequency, is inconsistent with the scaling result because c/ω_{pe} is proportional to $n_e^{-0.5}$ whereas W is proportional to $n_e^{0.2}$. It is also inconsistent with the B_T scaling result that W is strongly dependent on B_T, since c/ω_{pe} is independent of B_T.

In the usual theory of electromagnetic drift wave turbulence,[10] one has

$$W^{dw} \simeq 3\rho_s,$$

and

$$b_0^{dw} \simeq 3\beta \frac{\rho_s}{L_n}.$$

Here, the superscript "dw" denotes drift wave turbulence Also, $\rho_s = c_s/\Omega_i$, $c_s = \sqrt{T_e/M_i}$, Ω_i is the ion gyrofrequency, M_i is the ion mass, $\beta = 8\pi p_o/B_T^2$, and $L_n = -\left[d\ln n_e/dr\right]^{-1}$. Although theory correctly predicts the B_T scaling, b_0^{dw} is about 1/10 of b_0. Also, because β is lower at the edge of the plasma, b_0^{dw} at the edge is smaller than b_0^{dw} at the $q = 2$ surface, in disagreement with the fact that b_0 must be larger at the edge in order to account for the radially increasing χ_e. Furthermore, τ_R and τ_E increase sharply at the onset of the H-mode (Fig. 8) while β_p also increases further, due to improved global confinement. This indicates that the high level of magnetic turbulence in the L-mode is not a trivial consequence of increasing β_p, in contradiction with the prediction of simple electromagnetic drift wave turbulence theory.

We now investigate the three resistive MHD instabilities.[19] Rippling modes,[20] or current convective instabilities, are excited by a resistivity gradient and a parallel equilibrium current in Ohm's law and are stabilized by a large parallel thermal conductivity. A nonlinear study shows that

$$W^{ripp} = \left(c\frac{E_0 L_s}{B_0 L_\eta}\right)^{\frac{1}{3}} (\chi_\parallel \overline{k}_\parallel'^2)^{-\frac{1}{3}}.$$

Here, the superscript "ripp" denotes rippling modes, E_0 is the equilibrium electric field, η is the resistivity, $L_\eta = \left[d\ln\eta/dr\right]^{-1}$, $k_\parallel' = k_\theta/L_s$, and $\chi_\parallel$ is the parallel thermal conductivity. One can then find b_0 by integrating Ohm's law around the rational surface and using the constant-Ψ approximation,[19] which yields

$$b_0^{ripp} = \frac{2\pi}{c}\frac{E_0}{\eta B_0}\left(c\frac{E_0 L_s}{B_0 L_\eta}\right)^{\frac{2}{3}} (\chi_\parallel \overline{k}_\parallel'^2)^{-\frac{2}{3}}.$$

Calculations show that W^{ripp} agrees with W, both in magnitude and in scalings. However, b_0^{ripp} is smaller than b_0 by a factor of 10^{-2}, which makes transport due to magnetic fluctuations induced by rippling modes insignificant.

Microtearing modes[21] are driven by an electron temperature gradient and the time-dependent thermal force. These modes have frequencies comparable to the diamagnetic drift frequency, ω_{*e}, and can be separated into two regimes according to the electron

response: collisional for adiabatic electrons ($\omega \gg \chi_{\|} k_{\|}^2$), and semicollisional for isothermal electrons ($\omega \ll \chi_{\|} k_{\|}^2$). The width of the thermal conduction layer determines $W^{\mu t}$:

$$W^{\mu t} = \left(\frac{\nu_e L_s}{\Omega_e L_{Te}}\right)^{\frac{1}{2}} (L_s \overline{k}_\theta^{-1})^{\frac{1}{2}}.$$

Here, the superscript "μt" denotes microtearing modes, ν_e is the electron collision rate, and $L_{Te} = -[d \ln T_e / dr]^{-1}$. When $W^{\mu t}$ is comparable to the width of the magnetic island, one finds

$$b_0^{\mu t} = \frac{\nu_e L_s}{\Omega_e L_{Te}}.$$

With ASDEX parameters, $W^{\mu t}$ is in agreement with W and is consistent with scaling results. This correctly predicts the radially increasing χ_e, since $b_0^{\mu t}$ at the edge is larger than $b_0^{\mu t}$ at the $q = 2$ surface, because of the low edge temperature. Its magnitude also agrees with b_0 as observed in the OH-mode. However, microtearing modes do not seem to be a viable candidate because the magnitude of $b_0^{\mu t}$ is about 1/10 that of b_0 in the L-mode.

Resistive-ballooning modes[22] are excited by a pressure gradient in the bad curvature region, when β_p is large in spite of the average minimum-B configuration of the tokamak. These are the toroidal analog of resistive interchange modes. Since field line bending is a dominant stabilizing force, one finds W^{rb} by balancing inertia with field line bending to obtain

$$W^{rb} = \frac{\overline{k}_\theta q}{\hat{s}} \left[\hat{s} n^2 \gamma_n \tau_A / S_M\right]^{\frac{1}{4}}.$$

Here, the superscript "rb" denotes resistive-ballooning modes and S_M is the ratio of the resistive time τ_r to the poloidal Alfvén time τ_A with $\tau_A = Rq/v_A$ where v_A is the Alfvén speed. The growth rate, γ_n, is given by

$$\gamma_n = \left(\beta_p \epsilon \frac{r}{L_p}\right)^{\frac{2}{3}} \left(\frac{n^2}{S_M}\right)^{\frac{1}{3}} \tau_A^{-1}.$$

Here, ϵ is the inverse aspect ratio and $L_p = -[d \ln p / dr]^{-1}$, where p is the pressure. Using Ohm's law and Ampere's law, one finds

$$b_0 = \frac{4\pi}{c^2} \frac{\overline{k}_\theta}{\eta L_s} \left(W^{rb}\right)^4 \gamma_n.$$

For ASDEX, W^{rb} agrees well with W in magnitude and scalings. Also, b_0^{rb} is consistent with radially increasing χ_e and the observed confinement degradation during NBI. Although the n_e and B_T dependence of b_0^{rb} is somewhat stronger than that indicated by the parameter scan, resistive-ballooning modes seem to offer the most plausible explanation of the results.

It is interesting to note that a recent study[23] of the effect of a diverted tokamak geometry shows that, because of increased shear near the separatrix, resistive MHD modes can be quenched, thus leading to a transport barrier[24] and good confinement behavior in the H-mode. It is also interesting to note that because W^{rb} and b_0^{rb} are strongly dependent on m, an accurate measurement of $\overline{m}$ may reveal that W^{rb} and b^{rb} are considerably larger or smaller than indicated by the present calculations. However, we note that scalings as well as relative magnitudes at different positions (i.e., b_0 at $q = 2$ must be smaller than b_0 at the edge to match with the radially increasing χ_e) and in different operational regimes (i.e., b_0 in the L-mode must be larger than b_0 in the OH-mode to be consistent with confinement degradation during auxiliary heating) are more important than the magnitude itself in determining the consistency of theories.

Finally, Alfvénic microturbulence is also a plausible candidate since it has a characteristic radial scale length that is comparable to the Alfvén layer width, $x_A = \rho_s c_S L_S / L_n v_A$. Note that x_A is proportional to $n_e^{\frac{1}{2}} B_T^{-1}$, consistent with the n_e and B_T scan results. Further, detailed experimental results are needed to distinguish between the various possibilities.

V. Conclusions

We have derived a simple theory for χ_e, which enables us to calculate the radial correlation length, W, of the electromagnetic turbulence from the ratio of τ_R/τ_E. Then b_0 can also be determined by matching the experimantally deduced χ_e, if $\overline{m}$ is known. This electromagnetic microturbulence seems to govern τ_R and τ_E simultaneously in the L-mode, as evidenced by the clear correlation in confinement properties. Scalings of W and b_0 are deduced from parameter scans. These properties of microturbulence are compared with various theoretical predictions in order to test the consistency of theories.

The principal results are as follows:

(i) From the ratio of τ_R/τ_E, we calculate W to be about 1 mm, independent of assumptions about confinement zones or modelling.

(ii) With the assumption that $\overline{m}$ is $6 \sim 10$ and that the radial stucture of the underlying magnetic turbulence is nearly Gaussian, b_0 is estimated to be about 2×10^{-4} at the edge of the typical L-mode plasma. This result is in agreement with the level which is experimentally deduced from measurements outside the separatrix.[25]

(iii) From plasma parameter scanning results, we find

$$W \sim n_e^{0.2} B_T^{-1.3} P^{0.05} \quad \text{and} \quad b_0 \sim n_e^{-0.05} B_T^{-0.6} P^{0.6}.$$

(iv) Among various turbulence theories, the skin-depth turbulence theory[18] is in contradiction with our scan results, since c/ω_{pe} is proportional to $n_e^{-0.5}$. Rippling[20] and microtearing[21] modes predict magnetic fluctuation levels that are too low to explain the observed χ_e in the L-mode. Resistive-ballooning modes[22] seem to be the candidate which is most consistent, in both magnitude and scalings, with the data.

Acknowledgements

The authors acknowledge their gratitude to C. W. Barnes, D. Robinson, B. A. Carreras, J. L. Dunlap, M. Murakami, J. Harris, F. Holzhauer, and S. J. Zweben for stimulating discussions. One of us (O.J.K.) would like to thank N. Mattor for his comments on the manuscript.

This research was supported by the United States Department of Energy under Contract No. DE-FG05-80ET-53088.

Appendix

In this Appendix, it is shown that electrostatic turbulence cannot simultaneously underlie τ_R and τ_E in the ASDEX tokamak. To do this, we first assume that heat transport of both REs and bulk plasma is due to electrostatic turbulence and later we will show that this assumption leads to unphysical implications. For simplicity, only the electrostatic weak turbulence regime is considered here.

Starting from the electrostatic electron drift kinetic equation for untrapped electrons, one finds χ_e by following the same steps described in Sec.III-A:

$$\chi_e = \pi \left(\frac{cT_e}{eB_0}\right)^2 \sum_{\mathbf{k},\omega} k_\theta^2 |\frac{e\tilde{\phi}_{\mathbf{k},\omega}}{T_e}|^2 \delta(\omega - \omega_D - k_\parallel v_\parallel). \qquad (A-1)$$

Here, $\tilde{\phi}$ is the fluctuating electrostatic potential. The spectrum of $\tilde{\phi}$ can be written as

$$|\frac{e\tilde{\phi}_{\mathbf{k},\omega}}{T_e}|^2 = \frac{\phi_0^2}{W_{mI}^{ES} I^{ES}} F^{ES}(m) S_{\mathbf{k}}^{ES} \left(\frac{x}{W_m^{ES}}\right) \frac{\delta\omega_{\mathbf{k}}}{\pi\left[(\omega-\omega_{\mathbf{k}})^2 + \delta\omega_{\mathbf{k}}\right]}. \qquad (A-2)$$

Here, the superscript "ES" denotes electrostatic turbulence and

$$\phi_0^2 = \sum_{\mathbf{k},\omega} |\frac{e\tilde{\phi}_{\mathbf{k},\omega}}{T_e}|^2. \qquad (A-3)$$

Equations (A-2) and (A-3) can be compared with Eqs. (13) and (11), respectively, and W_{mI}^{ES}, F^{ES}, $S_{\mathbf{k}}^{ES}$ and I^{ES} have same meanings as before, with the replacement of "electrostatic" with "magnetic". Since the ballistic frequency dominates for thermal electrons, we have

$$\chi_{e,Th} = \frac{\pi \bar{k}_\theta L_s}{\overline{W}_{mI}^{ES} v_{\parallel,Th}} \left(\frac{cT_e}{eB_0}\right)^2 \phi_0^2. \qquad (A-4)$$

However, because of the large drift velocity across magnetic field lines for REs, we find

$$\chi_{e,R} = \frac{\pi \bar{k}_\theta L_s}{\overline{W}_{mI}^{ES} v_{\parallel,R}} \left(\frac{cT_e}{eB_0}\right)^2 \phi_0^2 S_{\mathbf{k}}^{ES} \left(\frac{\omega_{D,R}}{\bar{k}'_\parallel v_{\parallel,R} \overline{W}_m^{ES}}\right). \qquad (A-5)$$

Then, comparing Eq. (A-5) with Eq. (A-4), one finds

$$S_{\mathbf{k}}^{ES} \left(\frac{\omega_{D,R}}{\bar{k}'_\parallel v_{\parallel,R} \overline{W}_m^{ES}}\right) = \frac{\tau_E v_{\parallel,R}}{\tau_R v_{\parallel,Th}}. \qquad (A-6)$$

For typical parameters, the right-hand side of Eq. (A-6) is about 10, which is unphysical because these modes are well localized around the rational surface, which implies $S_{\mathbf{k}} \leq 1$.

References

1. H. P. Furth, Nucl. Fusion **15**, 487 (1975).
2. S. P. Hirshman and D. J. Sigmar, Nucl. Fusion **21**, 1079 (1981); F. L. Hinton and R. D. Hazeltine, Rev. Mod. Phys. **48**, 239 (1976).
3. P. C. Liewer, Nucl. Fusion **25**, 543 (1985); W. M. Tang, Nucl. Fusion **18**, 1089 (1978).
4. J. D. Callen, Phys. Rev. Lett. **39**, 1540 (1977).
5. A. B. Rechester and M. N. Rosenbluth, Phys. Rev. Lett. **40**, 38 (1978).
6. T. H. Stix, Nucl. Fusion **18**, 353 (1978); J. A. Krommes, C. Oberman, and R. G. Kleva, J. Plasma Physics **30**, 11 (1983); B. B. Kadomtsev and O. P. Pogutse, in *Plasma Physics and Controlled Nuclear Fusion Research* 1978 (IAEA, Vienna, 1979), Vol. 1, p. 649.
7. H. E. Mynick and J. D. Strachan, Phys. Fluids **24**, 695 (1981).
8. H. E. Mynick and J. A. Krommes, Phys. Fluids **23**, 1229 (1980); H. E. Mynick and J. A. Krommes, Phys. Rev. Lett. **43**, 1506 (1979).
9. H. Dreicer, Phys. Rev. **115**, 238 (1959).
10. F. Wagner, G. Becker, et al., Phys. Rev. Lett. **49**, 1408 (1982); S. M. Kaye et al., J. Nucl. Mater. **121**, 115 (1984); N. Ohyabu et al., Nucl. Fusion **25**, 49 (1985).
11. P. W. Terry and P. H. Diamond, Phys. Fluids **28**, 1419 (1985); P. W. Terry and W. Horton, Phys. Fluids **26**, 106 (1983); R. E. Waltz and R. R. Dominguez, Phys. Fluids **26**, 3338 (1983).
12. C. W. Barnes, Ph.D. Thesis, Princeton University, 1981.
13. T. M. Antonsen and B. Lane, Phys. Fluids **23**, 1205 (1980); P. J. Catto, W. M. Tang, and D. E. Baldwin, Plasma Phys. **23**, 639 (1981).
14. F. W. Perkins, in *Heatings in Toroidal Plasmas* (Proc. 4th Int. Symp. Rome, 1984), Vol. 2 (1984) p. 977.
15. H. P. Furth, Bull. Am. Phys. Soc. **30**, 1386 (1985).

16. F. Wagner, G. Becker, et al., in *Plasma Physics and Controlled Nuclear Fusion Research* 1982 (IAEA, Vienna, 1983), Vol. 1, p. 43.

17. J. L. Dunlap, private communication; see also N. Ohyabu, G. L. Jahns, R. D. Stambaugh, and E. J. Strait, Phys. Rev. Lett. **58**, 120 (1987).

18. B. B. Kadomtsev and O. P. Pogutse, in *Plasma Physics and Controlled Nuclear Fusion Research* 1984 (IAEA, Vienna, 1985), Vol. 2, p. 69; B. B. Kadomtsev and O. P. Pogutse, Sov. Phys.-JETP Lett. **39**, 269 (1984).

19. H. P. Furth, J. Killeen, and M. N. Rosenbluth, Phys. Fluids **6**, 459 (1963).

20. L. Garcia, P. H. Diamond, B. A. Carreras, and J. D. Callen, Phys. Fluids **28**, 2147 (1985); J. D. Callen et al., in *Plasma Physics and Controlled Nuclear Fusion Research* 1982 (IAEA, Vienna, 1983), Vol. 1. p. 297.

21. N. T. Gladd, J. F. Drake, et al., Phys. Fluids **23**, 1182 (1980); J. F. Drake and Y. C. Lee, Phys. Fluids **20**, 1341 (1977).

22. B. A. Carreras, P. H. Diamond, et al., Phys. Rev. Lett. **49**, 1408 (1982); P. H. Diamond et al., Phys. Fluids **27**, 1116 (1985); J. F. Drake and T. M. Antonsen, Jr., Phys. Fluids **28**, 544 (1985).

23. T. S. Hahm and P. H. Diamond, Phys. Fluids **30**, 133 (1987).

24. F. Wagner, G. Fussman, et al., Phys. Rev. Lett. **53**, 1453 (1984).

25. F. Holzhauer, private communication.

Figure Captions

Fig. 1 Runaway electron drift orbit (solid line) shifted outward with respect to the magnetic separatrix (dashed line).

Fig. 2 Time evolution of hard X-ray signal ϕ_x during the OH-mode interrupted by two sequential neutral beam injection (NBI) pulses. NBI phases are indicated by hatched time intervals.

Fig. 3 Time evolution of (a) plasma current I_P, central chord-averaged electron density $\overline{n}_e$, and loop voltage V_L and (b) ϕ_x during the initial and current ramp-up phases.

Fig. 4 Comparision of energy confinement time τ_E (open squares) and runaway electron confinement time τ_R (closed squares) in an ohmic B_T-scan.

Fig. 5 Time evolution of (a) ϕ_x and I_P in the OH-mode and (b) ϕ_x in the L-mode. NBI phase is indicated by the hatched time interval.

Fig. 6 Power dependence of τ_E (open rectangles), particle confinement time τ_P (asterisks), and τ_R (open circles) normalized to their OH-values.

Fig. 7 τ_R in a q_a (or B_T) scan in the L-mode. τ_E is independent of q_a in this phase.

Fig. 8 Time evolution of (a) $\overline{n}_e$, (b) ϕ_x, (c) H_α-radiation, (d) back-reflected flux ϕ_a from the neutralized plate, in the OH-, L-, and H-modes. The transition from the L- to the H-mode is indicated by the dashed vertical line.

Fig. 9 n_e-dependence of τ_E in the OH-mode (open squares) and the L-mode (open triangles) and of τ_R in the L-mode (closed squares).

Table 1

$W\ (mm)$				$b_0\ (10^{-4})$			
OH-mode		L-mode		OH-mode		L-mode	
$q=2$	edge	$q=2$	edge	$q=2$	edge	$q=2$	edge
1.3	1.1	1.3	1.2	0.48	0.87	1.1	1.8

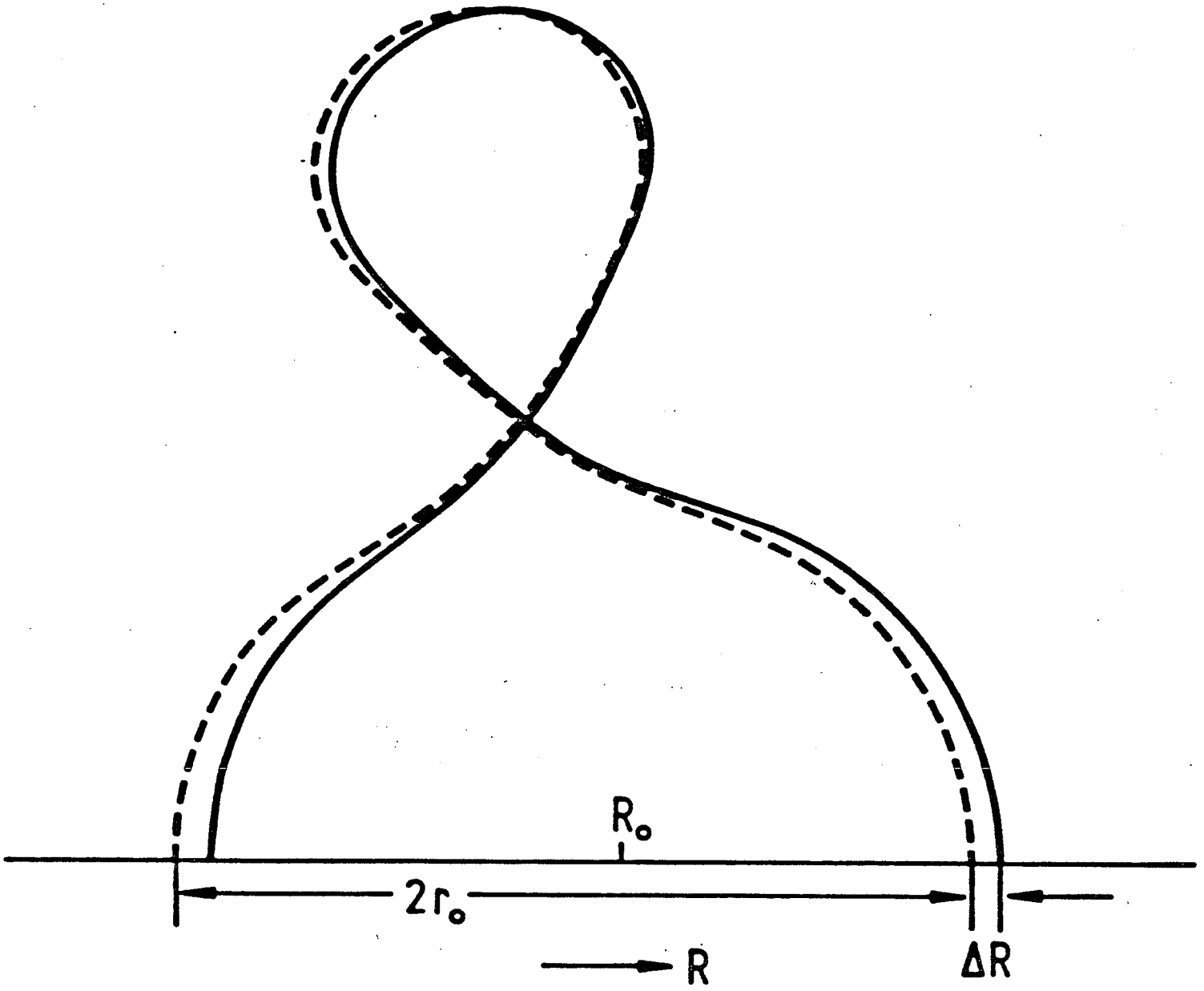

Fig. 1

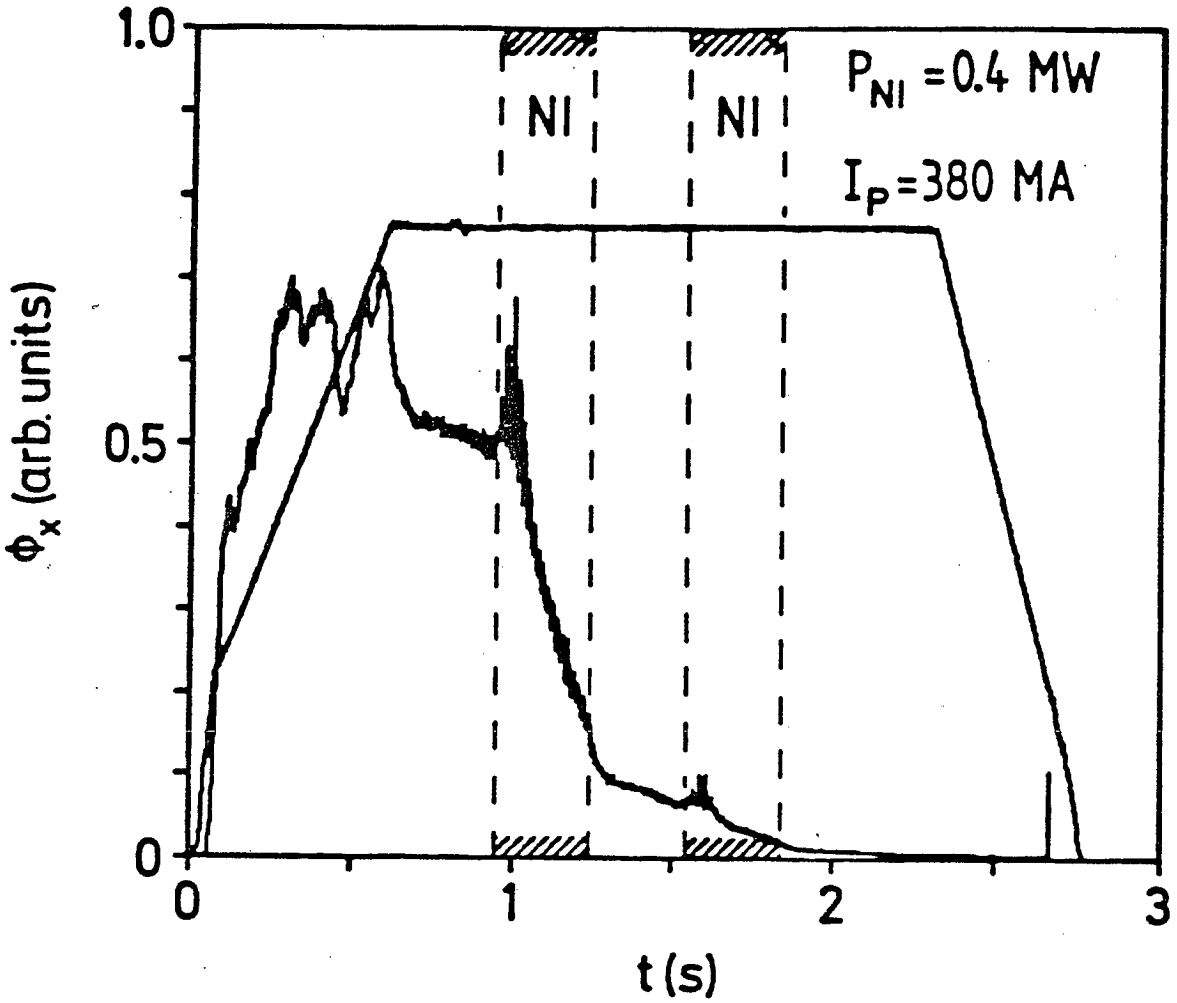

Fig. 2

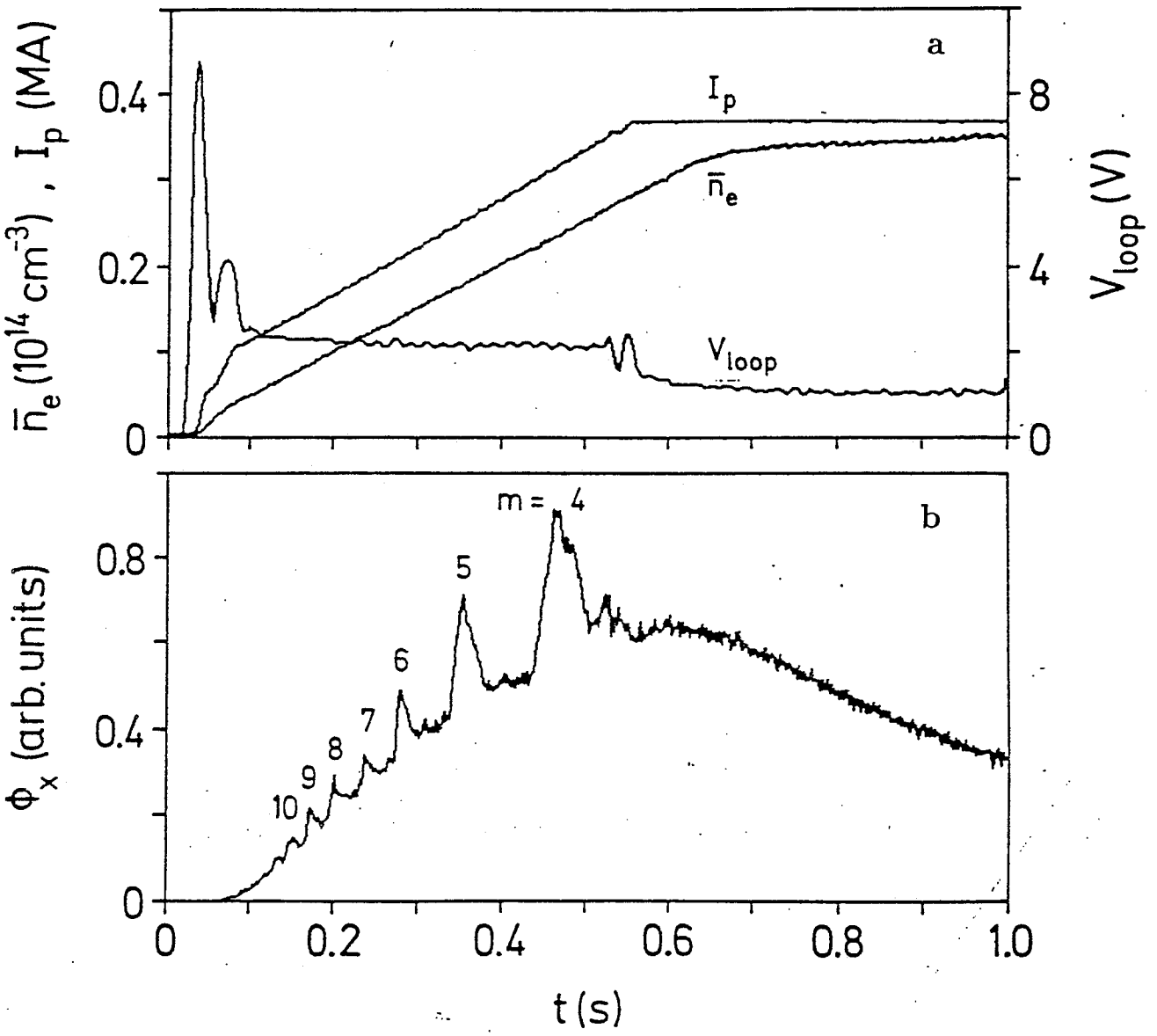
a
I_p
$\bar{n}_e$
V_{loop}
$\bar{n}_e\,(10^{14}\,cm^{-3})$, I_p (MA)
V_{loop} (V)
0.4
0.2
0
8
4
0
b
m = 4
5
6
7
8
9
10
ϕ_x (arb. units)
0.8
0.4
0
0
0.2
0.4
0.6
0.8
1.0
t (s)

Fig. 3

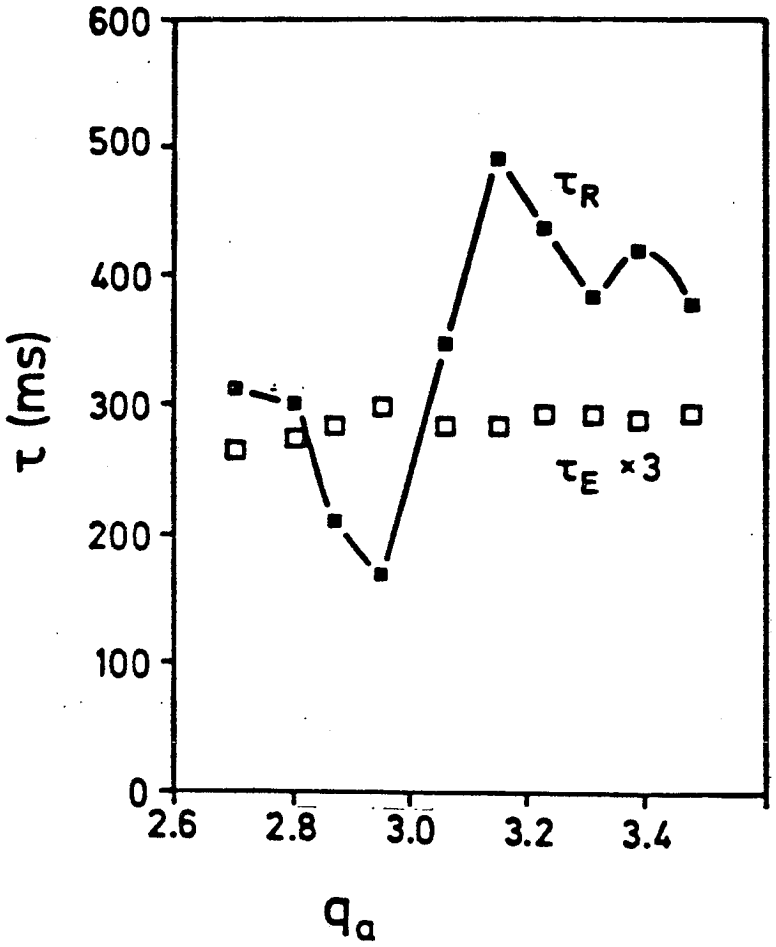

Fig. 4

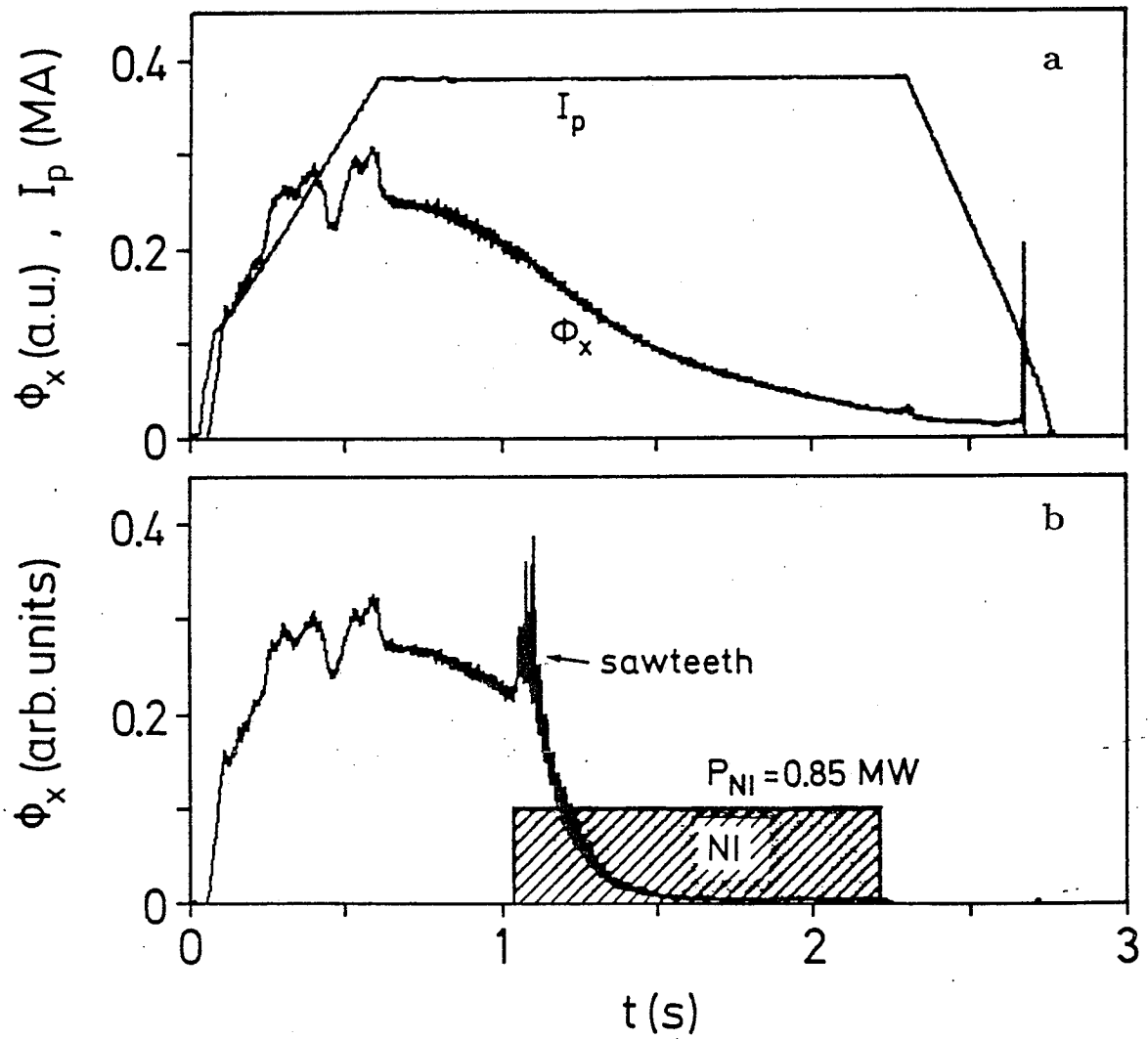
a
b
I_p
Φ_x
sawteeth
P_{NI} = 0.85 MW
NI
ϕ_x (a.u.) , I_p (MA)
ϕ_x (arb. units)
0.4
0.2
0
0
1
2
3
t (s)

Fig. 5

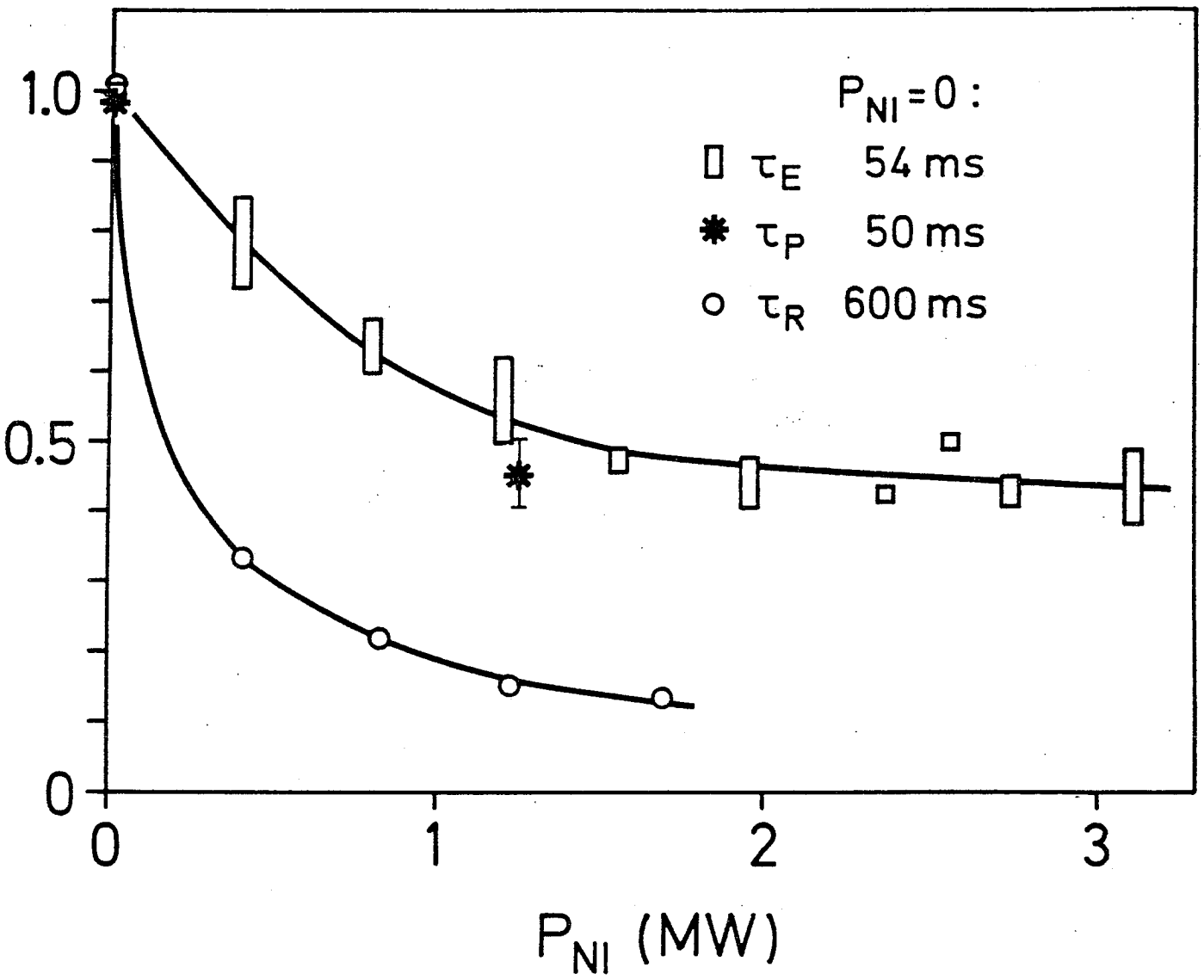

Fig. 6

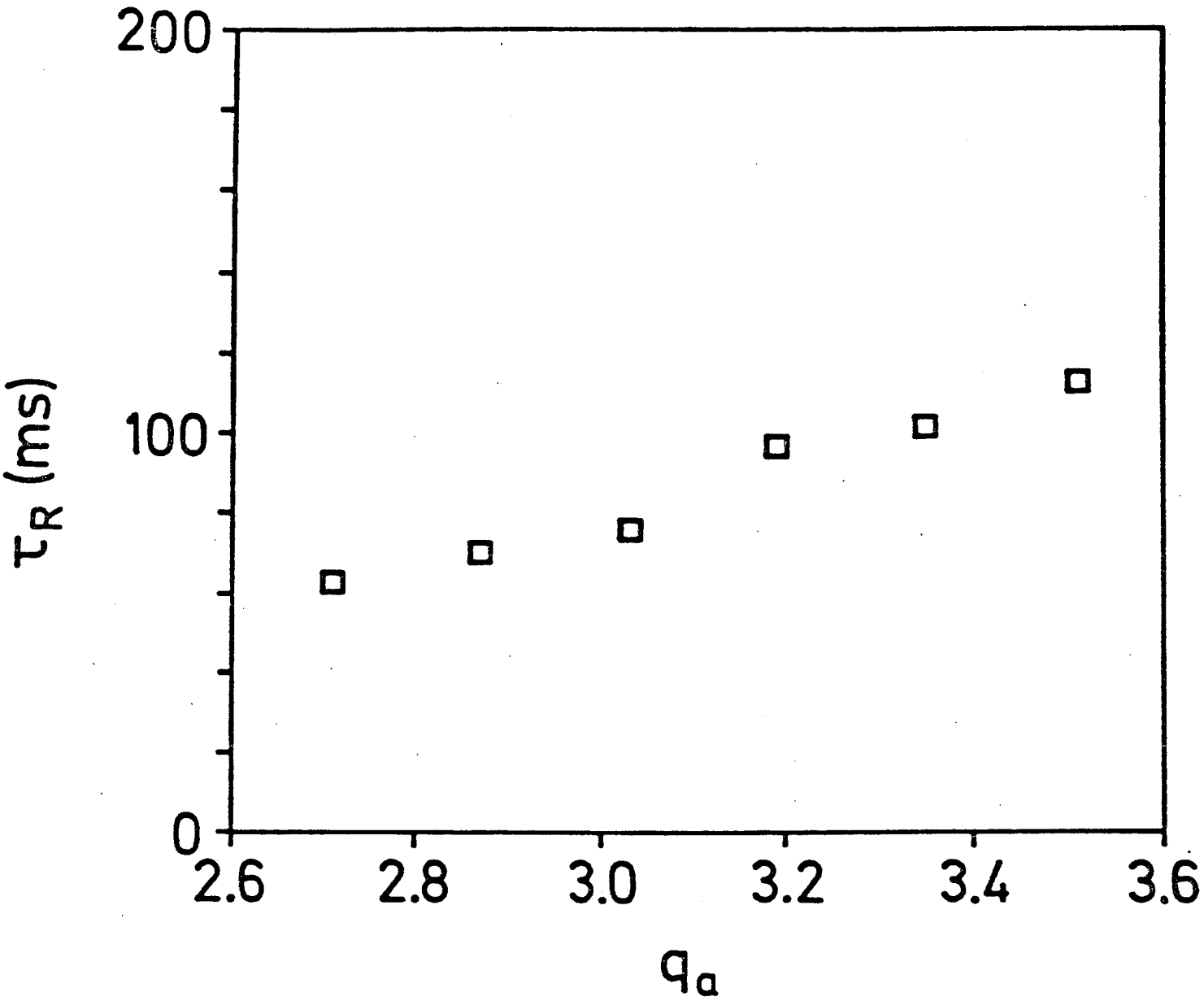

Fig. 7

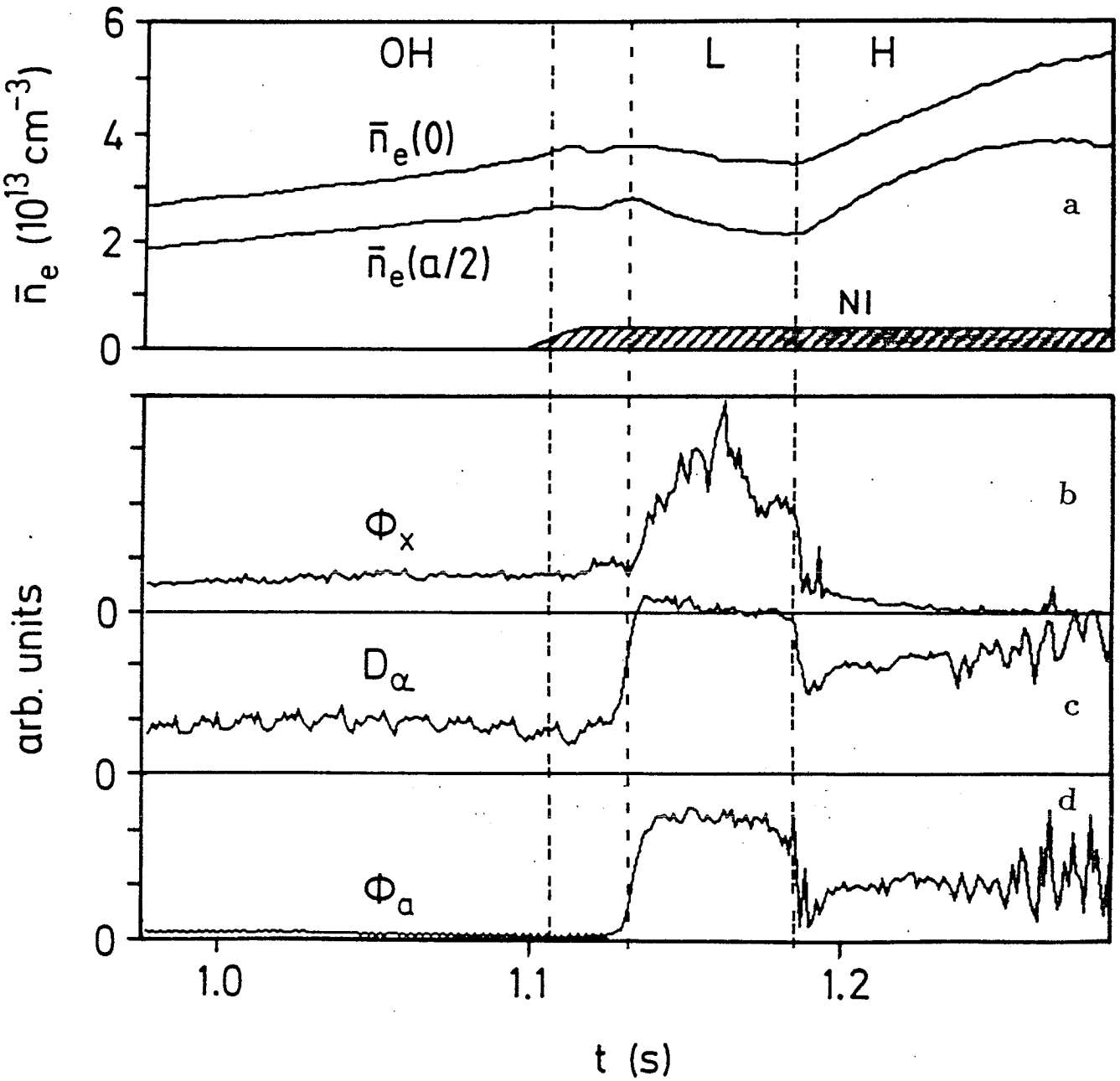
6
4
2
0
OH
L
H
$\bar{n}_e(0)$
$\bar{n}_e(a/2)$
a
NI
$\bar{n}_e$ (10^{13} cm^{-3})
b
Φ_x
0
D_α
c
0
d
Φ_a
0
arb. units
1.0
1.1
1.2
t (s)

Fig. 8

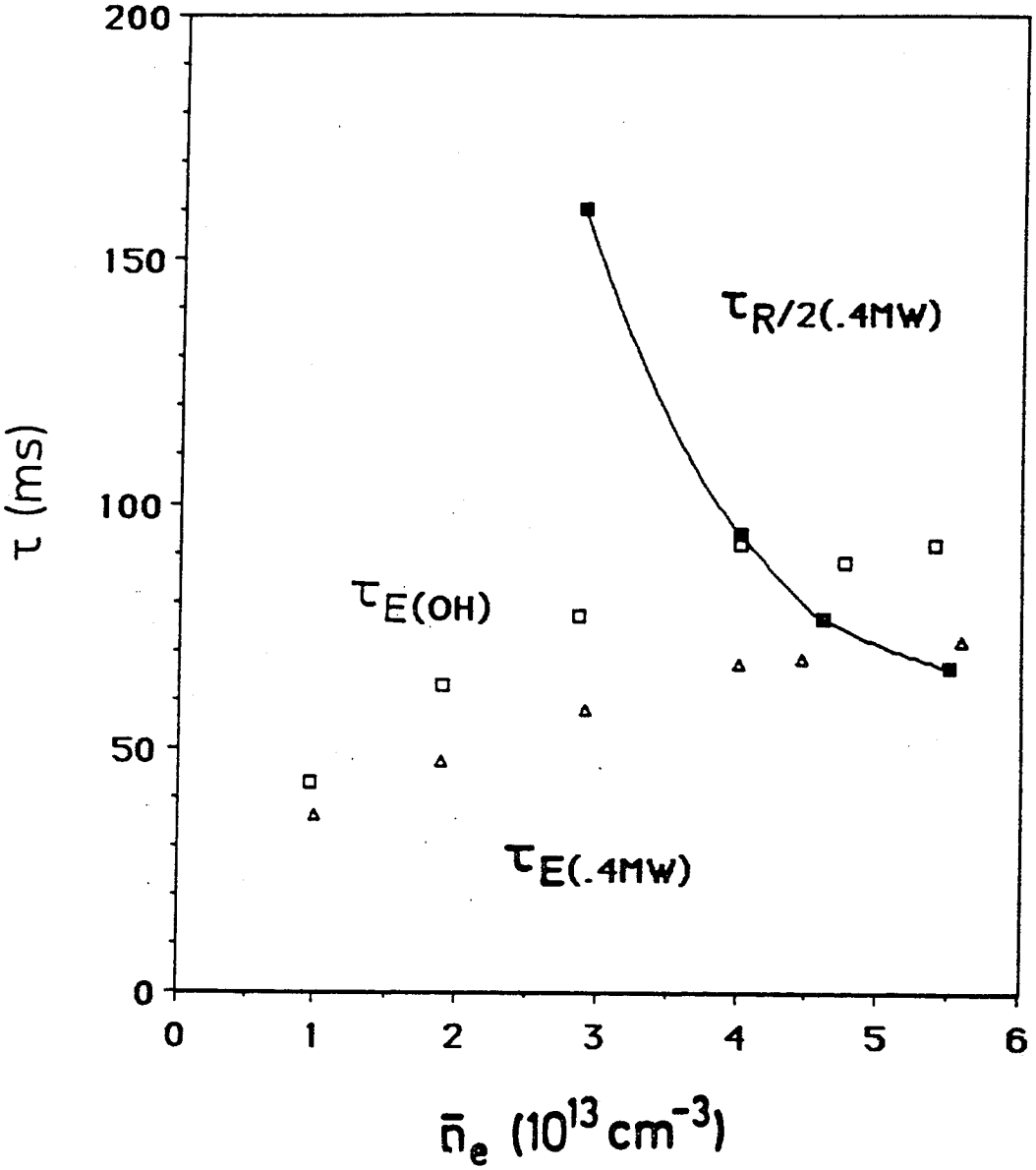

Fig. 9